Multipartite entanglement generation with dipole induced transparency effect in indirectly coupled dipole-microcavity systems

Zhaohui Peng (彭朝晖)[1,*], Chunxia Jia (贾春霞)[1,2], Yuqing Zhang (张玉青)[1], Zhonghua Zhu (朱中华)[1], and Xiaojuan Liu (刘小娟)[1]

[1]*Institute of Modern Physics and Department of Physics, Hunan University of Science and Technology, Xiangtan 411201, China*

[2]*Key Laboratory of Low-Dimensional Quantum Structures and Quantum Control of Ministry of Education, Department of Physics, Hunan Normal University, Changsha 410081, China*

*Corresponding author: raul121991@126.com

We propose a feasible scheme of generating multipartite entanglement with the dipole induced transparency (DIT) effect in indirectly coupled dipole-microcavity systems. It is shown that the transmission spectrum is closely related with the interference of dipole-microcavity systems, and we can generate different classes of multipartite entanglement, e.g., the Greenberger–Horne–Zeilinger state, the W state, and the Dicke state, of the dipole emitters just by choosing an appropriate frequency of the incident photon. Benefiting from the DIT effect, the schemes may work in the bad or low-Q cavity regime only if the large Purcell factor of the dipole-microcavity system is fulfilled, and they are also insensitive to experimental noise, which may be feasible with present accessible technology.

OCIS codes: 270.5580, 270.5585.
doi: 10.3788/COL201816.082702.

Multipartite entanglement has been widely regarded as the essential ingredient for implementing novel quantum information processing (QIP) tasks, such as controlled teleportation[1], quantum secret sharing[2], and universal error correction[3,4]. Dür *et al.*[5] have shown that there are two inequivalent classes of tripartite entangled states, i.e., the Greenberger–Horne–Zeilinger (GHZ) class and the W class. An important property of the W state is that it is robust against the loss of qubits, and it can still be used as a resource even if one of the qubits is lost. The Dicke state of n particles and k excitations, $|D_{n,k}\rangle = \sum \hat{P}_n^k (|0\rangle^{\otimes(n-k)}|1\rangle^{\otimes k})/\sqrt{C_n^k}$, is another important class of multipartite entangled state[6], and it exhibits genuine many-body entanglement[7] and resists against decoherence, particle loss, and measurement[8]. Local operations performed on any constituent particle can not destroy all of the entanglement shared by the other particles[9], and thus, the Dicke state might be interesting from the view of QIP between many participants.

Solid state qubits have many promising properties, such as large scalability, long coherence time, and optical addressability, and have already been realized with semiconductor quantum dots[10] and nitrogen-vacancy (NV) centers in diamond[11]. Quantum entanglement of solid state qubits is the fundamental resource in scalable QIP and quantum computation, and optical excitation of solid state qubits may be the best choice to generate entanglement in a scalable way. However, the strong coupling between solid state qubits and photons may be challenging with the present experimental technology.

Fortunately, Waks and Vuckovic proposed the dipole induced transparency (DIT) effect[12], and then experimentally demonstrated this effect in the photonic crystal cavity-waveguide system[13]. The distinct advantage of the DIT effect is that it can be realized in the dipole-microcavity system with a large Purcell factor; thus, it allows the system to work in the bad cavity regime, which greatly relaxes the experimental requirement of the system. On the other hand, whispering-gallery-mode (WGM) microcavities[14–17] with an ultrahigh quality factor are experimentally feasible, and thus, a large Purcell factor of the system may be achievable for realizing the DIT effect. If we consider the polarization degree of freedom of the incident photon, the DIT effect can be utilized to modulate both the amplitude and phase of the incident photon. The amplitude modulation feature is useful for splitting a polarized light beam and functions as polarized beam splitter or photonic Stern–Gerlach apparatus[18], which may be tailored for generating spatial entanglement of photons and related QIP[19]. For perfect transmission or reflection, the conditional phase shift or photonic Faraday rotation[20] can be obtained, which may also be useful for QIP[21–24] and quantum computation[25,26].

Up to now, many entanglement generation schemes have been proposed in the dipole-microcavity system[27–30], whereas most of them have discarded the interference effect between the cascaded systems. In this Letter, we demonstrate that the interference effect between cascaded dipole-microcavity systems is of great importance for its transmission spectrum; then, we propose the schemes for

generating the GHZ state, W state, and Dicke state of the dipole emitters just by choosing an appropriate frequency of the incident photon. Benefiting from the DIT effect, the schemes can be achievable with less demanding technology of the cavity-quantum electrodynamics (QED) system, and they are also insensitive to experimental noises, e.g., spontaneous emission of the dipole emitter and photon loss in the microcavity and waveguide. Moreover, the schemes can be extended to generate N-qubit entanglement straightforwardly.

The schematic of entanglement generation is depicted in Fig. 1(b), where three dipole-microcavity systems are evanescently coupled to two drop-filter waveguides, respectively. The dipole emitter has two degenerate ground states and one excited state, as shown in Fig. 1(a), and the logic qubits of dipole emitters $\{|0\rangle, |1\rangle\}$ are encoded in their ground states $\{|g_L\rangle, |g_R\rangle\}$. The microcavities are assumed to have a single mode $a_i (i = 1, 2, 3)$ that couples only to the forward propagating fields. The dipole emitters with transition frequencies ω_{ai} are evanescently coupled to the corresponding microcavities, respectively, and their interaction can be descried by the Jaynes–Cummings model Hamiltonian. The Heisenberg–Langevin equations of cavity modes a_i and dipole lower operators σ_{i-} are ($\hbar = 1$)

$$
\frac{\mathrm{d}a_i(t)}{\mathrm{d}t} = -i(\omega_i - \omega_p)a_i(t) - \frac{\kappa_1 + \kappa_2 + \kappa_0}{2}a_i(t) - g_i\sigma_{i-}(t)
$$
$$
- \sqrt{\kappa_1}a_{i,\mathrm{in}}(t) - \sqrt{\kappa_2}e^{i\phi_i}a_{i+1,\mathrm{out}}(t),
$$
(1)

$$
\frac{\mathrm{d}\sigma_{i-}(t)}{\mathrm{d}t} = -i(\omega_{ai} - \omega_p)\sigma_{i-}(t) - \frac{\gamma_{ai}}{2}\sigma_{i-}(t) - g_i a_i(t)\sigma_{iz}(t)
$$
$$
+ \sqrt{\gamma_{ai}}\sigma_{iz}(t)b_{i,\mathrm{in}}(t),
$$
(2)

where ω_p, ω_i are the frequency of the input field and the central frequency of the ith microcavity. $\kappa_i (i = 1, 2)$ is the cavity-waveguide coupling strength, and κ_0 is the intrinsic loss of microcavity. $a_{i,\mathrm{in}}$ and $a_{i,\mathrm{out}}$ describe the input and output fields of the ith microcavity. ϕ_i denotes phase delay along the waveguides between microcavities, and we set $\exp(i\phi_i) = 1$ by choosing an appropriate distance of
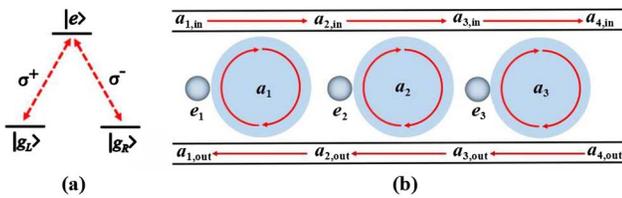
Fig. 1. Schematic of generating multipartite entanglement of dipole emitters in three dipole-microcavity systems. (a) The energy-level configuration of the dipole emitter. The transition $|g_{L(R)}\rangle \leftrightarrow |e\rangle$ is driven by left (right) circularly polarized light. (b) Three indirectly coupled dipole-microcavity systems.

cavities. g_i and σ_{i-} are the vacuum Rabi frequency and lower operator of the ith dipole emitter. γ_{ai} and $b_{i,\mathrm{in}}(t)$ are the spontaneous emission rate of the dipole emitter and its noise input operator.

In what follows, we consider the weak excitation limit, and thus, all of the dipole emitters are always in their ground states, which allows us to replace the dipole population operator with its expectation value $\langle\sigma_{iz}\rangle \approx -1$[31]. Moreover, we assume that the external field of the dipole emitter is in the thermal equilibrium state, and the contribution of the noise input operator is negligible [i.e., $\langle b_{\mathrm{in}}(t)\rangle = 0$]. The output fields into the waveguides are related to the input fields by the input–output relations[32] $a_{i+1,\mathrm{in}}(t) = a_{i,\mathrm{in}}(t) + \sqrt{\kappa_1}a_i(t)$ and $a_{i,\mathrm{out}}(t) = a_{i+1,\mathrm{out}}(t) + \sqrt{\kappa_2}a_i(t)$. We assume that a weak monochromatic field with frequency ω_p inputs from the left port of the upper waveguide, as shown in Fig. 1(b) $[a_{4,\mathrm{out}}(t) = 0]$, and the output fields into the waveguides are given by $a_{4,\mathrm{in}}(t) = a_{1,\mathrm{in}}(t) + \sqrt{\kappa_1}\sum_{i=1}^{3}a_i(t)$ and $a_{1,\mathrm{out}}(t) = \sqrt{\kappa_2}\sum_{i=1}^{3}a_i(t)$. In the steady state, the field in the ith microcavity is $a_i(t) = D_i/D$, where

$$
D = \begin{vmatrix} i\Delta'_1 - \kappa/2 & -\kappa_2 & -\kappa_2 \\ -\kappa_1 & i\Delta'_2 - \kappa/2 & -\kappa_2 \\ -\kappa_1 & -\kappa_1 & i\Delta'_3 - \kappa/2 \end{vmatrix},
$$
(3)

and D_i is the determinant by replacing the ith column of D with $\sqrt{\kappa_1}a_{1,\mathrm{in}}(t)(1,1,1)^T$. The parameters of the systems are $\kappa = \kappa_0 + \kappa_1 + \kappa_2$, $\Delta_i = \omega_p - \omega_i$, $\Delta_{ai} = \omega_p - \omega_{ai}$, and $i\Delta'_i = i\Delta_i + g_i^2/(i\Delta_{ai} - \gamma_{ai}/2)$. Analog to the double-sided microcavity, we denote the output fields into upper and lower waveguides as transmission and reflection fields, respectively. We consider the critical coupling condition (i.e., $\kappa_1 = \kappa_2$) and can obtain the transmission and reflection coefficients as follows:

$$
T = \frac{a_{4,\mathrm{in}}(t)}{a_{1,\mathrm{in}}(t)} = \left[1 - \kappa_1 \sum_{i=1}^{3}(i\Delta'_i - \kappa_0/2)^{-1} \right]^{-1},
$$
(4)

$$
R = \frac{a_{1,\mathrm{out}}(t)}{a_{1,\mathrm{in}}(t)} = \frac{\kappa_1 \sum_{i=1}^{3}(i\Delta'_i - \kappa_0/2)^{-1}}{1 - \kappa_1 \sum_{i=1}^{3}(i\Delta'_i - \kappa_0/2)^{-1}}.
$$
(5)

The evolution of the system can be investigated through its reflection and transmission spectra, and the numerical calculation is based on Eqs. (4) and (5). We consider the case where the ith dipole emitter is resonantly coupling to the corresponding microcavity with the same coupling strength, and three microcavities are assumed to have the same central frequencies (i.e., $\omega_i = \omega_{ai}$, $\omega_1 = \omega_2 = \omega_3$, $g_i = g$). The cavity losses to waveguides are far larger than its intrinsic loss, and thus, it is reasonable to consider the limit $\kappa_1 \gg \kappa_0$. To facilitate the subsequent discussion but without loss of generality,

we assume that the Purcell factors of dipole-microcavity systems are far larger than 1 (e.g. $F_p = 2g^2/\kappa_1\gamma_a = 200$) when dipole emitters are coupling with the incident photon, while their Purcell factors are zero for the decoupling case. As three dipole-microcavity systems are indirectly coupled by waveguides, the interference between them may lead to the rich transparency phenomena. As shown in Eq. (4), the transmission coefficient evidently depends on the interference of the terms $\kappa_1(i\Delta'_i - \kappa_0/2)^{-1}$, which account for DIT effects of dipole-microcavity systems. In Fig. 2, it is shown that there are two sharp transparency windows in the transmission spectra $|T_1|^2$ (blue dotted) and $|T_2|^2$ (red dot-dashed). Moreover, the locations of transparency peaks have obvious shifts to the resonant regime, and the full width at half-maximum (FWHM) of the dip is obviously narrower than that of the DIT effect for single dipole-microcavity system, which can only result from the interference between dipole-microcavity systems. From the transmission spectra in Fig. 2, it is shown that the evolution of system is closely related with the frequency of the incident photon and can be divided into the following three cases.

• **Case (1)**. If the incident photon is resonant with all of the dipole-microcavity systems (i.e., $\omega_p = \omega_i = \omega_{ai}$), the transmission and reflection amplitudes are $|T_3| \approx 1 (|R_3| \approx 0)$ (black solid) and $|T_i| \approx 0 (|R_i| \approx 1)(i = 0, 1, 2)$, and the corresponding phases are $\phi_{T3} = 0$ and $\phi_{R0} = \phi_{R1} = \phi_{R2} = \pi$. If all of the dipole emitters are initially in the superposition state $|\psi_i\rangle = (|g_L^i\rangle + |g_R^i\rangle)/\sqrt{2}$, and the incident photon is in the linearly polarized state $|\psi_p\rangle = (|L\rangle + |R\rangle)/\sqrt{2}$, the system will evolve into

$$\frac{1}{4}|1\rangle(|+\rangle_p|\text{GHZ}^+\rangle + |-\rangle_p|\text{GHZ}^-\rangle) - \frac{\sqrt{6}}{4}|+\rangle_p|2\rangle|D_{3,1}\rangle -$$
$$\frac{1}{4}|2\rangle(|+\rangle_p|\text{GHZ}^+\rangle - |-\rangle_p|\text{GHZ}^-\rangle) - \frac{\sqrt{6}}{4}|+\rangle_p|2\rangle|D_{3,2}\rangle, \quad (6)$$
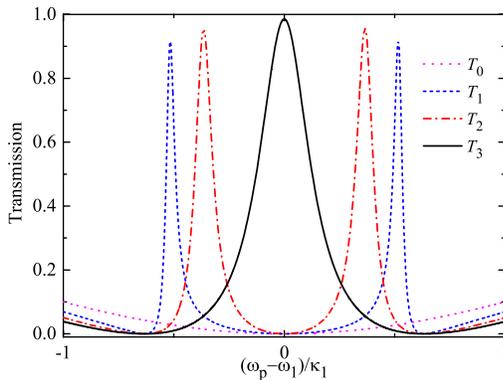
Fig. 2. Power transmission $|T_m|^2$ for three indirectly coupled dipole-microcavity systems with Purcell factor $F_p = 200$ of each system. T_m denotes the transmission coefficient in the case where the incident photon is coupling with m dipole emitters, respectively. The dipole-microcavity parameters $(g, \kappa_s, \gamma_a) = (0.33, 10^{-3}, 10^{-3})\kappa_1$ are taken into account.

where

$$|\pm\rangle_p = \frac{1}{\sqrt{2}}(|L\rangle \pm |R\rangle),$$

$$|\text{GHZ}^\pm\rangle = \frac{1}{\sqrt{2}}(|g_L^1\rangle|g_L^2\rangle|g_L^3\rangle \pm |g_R^1\rangle|g_R^2\rangle|g_R^3\rangle),$$

$$|D_{3,1}\rangle = \frac{1}{\sqrt{3}}(|g_L^1\rangle|g_L^2\rangle|g_R^3\rangle + |g_L^1\rangle|g_R^2\rangle|g_L^3\rangle + |g_R^1\rangle|g_L^2\rangle|g_L^3\rangle),$$

$$|D_{3,2}\rangle = \frac{1}{\sqrt{3}}(|g_L^1\rangle|g_R^2\rangle|g_R^3\rangle + |g_R^1\rangle|g_L^2\rangle|g_R^3\rangle + |g_R^1\rangle|g_R^2\rangle|g_L^3\rangle).$$

$$(7)$$

$|1\rangle$ and $|2\rangle$ denote the spatial states of the photon in the upper and lower waveguides, respectively. In the upper waveguide, the detection of the output photon in the basis $\{|\pm\rangle\}$ will lead to the GHZ state $|\text{GHZ}^\pm\rangle$ of the dipole emitters with the successful probability of 1/16, respectively. On the other hand, the detection of the output photonic state $|-\rangle$ in the lower waveguide leads to the GHZ state $|\text{GHZ}^+\rangle$ of dipole emitters. Thus, the total successful probability of generating the GHZ state is 3/16.

• **Case (2)**. If the frequency of the incident photon satisfies $\omega_p = \omega_1 \pm g/\sqrt{3}$, we can obtain the transmission and reflection amplitudes $|T_2| \approx 1 (|R_2| \approx 0)$ (red dot-dashed) and $|T_i| \approx 0 (|R_i| \approx 1)(i = 0, 1, 3)$. The corresponding phases are $\phi_{T2} = 0$ and $\phi_{R0} = \phi_{R1} = \phi_{R3} = \pi$. If all of the dipole emitters are initially in the superposition state $|\psi_i\rangle = (|g_L^i\rangle + |g_R^i\rangle)/\sqrt{2}$, and the incident photon is in the left circularly polarized state $|L\rangle$, the system evolves as

$$|L\rangle_p\left(\frac{\sqrt{6}}{4}|1\rangle|D_{3,1}\rangle + \frac{\sqrt{6}}{4}|2\rangle|D_{3,2}\rangle + \frac{1}{2}|2\rangle|\text{GHZ}^+\rangle\right). \quad (8)$$

Thus, the detection of the output photon in the upper waveguide yields the W state $|D_{3,1}\rangle$ of the dipole emitters with the successful probability of 3/8.

• **Case (3)**. If the frequency of the incident photon satisfies $\omega_p = \omega_1 \pm \sqrt{6}g/3$, the transmission and reflection amplitudes are $|T_1| \approx 1 (|R_1| \approx 0)$ (blue dotted) and $|T_i| \approx 0 (|R_i| \approx 1)(i = 0, 2, 3)$, and the corresponding phases are $\phi_{T1} = 0$ and $\phi_{R0} = \phi_{R2} = \phi_{R3} = \pi$. When the initial state of the system is just the same as that of case (2), the system evolves into

$$|L\rangle_p\left(\frac{\sqrt{6}}{4}|1\rangle|D_{3,2}\rangle + \frac{\sqrt{6}}{4}|2\rangle|D_{3,1}\rangle + \frac{1}{2}|2\rangle|\text{GHZ}^+\rangle\right). \quad (9)$$

The Dicke state of dipole emitters $|D_{3,2}\rangle$ can be obtained for the detection of the output photon in the upper waveguide, and the successful probability is 3/8.

We can extend the schemes straightforwardly to generate the N-qubit entanglement of dipole emitters by modifying the model to the case of N dipole-microcavity systems. If the weak excitation approximation for all of the dipole emitters is always valid, the transmission coefficient can be obtained with a similar procedure as $T_N = \left[1 - \kappa_1 \sum_{i=1}^{N}(i\Delta'_i - \kappa_0/2)^{-1}\right]^{-1}$. The transmission

amplitude is closely related with the interference of dipole-microcavity systems and the excitation number of the system; thus, we may generate the N-qubit ($N > 3$) GHZ state, W state, and Dicke state just by choosing an appropriate frequency of the incident photon as that of three-qubit case.

We briefly discuss the experimental feasibility of our schemes based on experimentally accessible technologies. The key element of our schemes is to realize indirectly coupled dipole-microcavity systems. The WGM microcavity and tapered fiber may be one of potential candidates for realizing this structure[33]. The NV center in diamond, which is evanescently coupled to a WGM microcavity, could be chosen as the dipole emitter; thus, the system for entanglement generation can be readily constructed with present experimental technology[34]. In the schemes, we have assumed that the incident photon will be completely transmitted or reflected in the case of a large Purcell factor without considering the noise of the system. However, there are still some sources of noise, e.g., spontaneous emission of the dipole emitter and photon loss in the microcavity and waveguide. After considering the experimental noise, the evolution of system in the realistic process may be approximately expressed as $|j\rangle|g_j\rangle|1\rangle \rightarrow T|j\rangle|g_j\rangle|1\rangle + R|j\rangle|g_j\rangle|2\rangle$. To evaluate the performance of the schemes, we calculate the fidelity defined as $F = |\langle\psi_{\text{real}}|\psi_{\text{ideal}}\rangle|^2$, where $|\psi_{\text{ideal}}\rangle$ and $|\psi_{\text{real}}\rangle$ are the output states of the system in the ideal and realistic cases, respectively. The fidelities of the GHZ state $|\text{GHZ}^\pm\rangle$, W state $|D_{3,1}\rangle$, and Dicke state $|D_{3,2}\rangle$ for the detection of the output photon in the upper waveguide (i.e., photonic state $|1\rangle$) are given by $F_{\text{GHZ}} = |T_3|^2$, $F_W = |T_2|^2$ and $F_{\text{Dicke}} = |T_1|^2$, respectively. The dipole-microcavity parameters $(\kappa_s, \gamma_a) = (10^{-3}, 10^{-3})\kappa_1$ are taken into account, and the ratio of g/κ_1 can determine the Purcell factor of the system. Therefore, the fidelities of entanglement are relevant to the Purcell factor of the system, and we plot the fidelities of entanglement against the Purcell factor of the dipole-microcavity system in Fig. 3. It is shown that the fidelities of three classes of entangled states
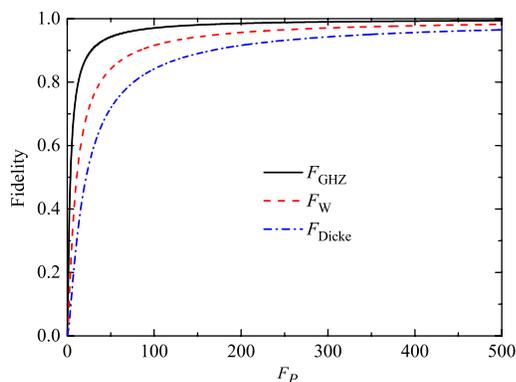
rapidly improve with the increase of the Purcell factor and gradually approach 1. For the same Purcell factor, they satisfy $F_{\text{GHZ}} > F_W > F_{\text{Dicke}}$, which reflects the fact that the transmission amplitude of the DIT effect is attributed to the overall Purcell factor of dipole-microcavity systems. The parameters of the dipole-microcavity system $(g, \kappa, \kappa_s, \gamma_a) = (180, 4.7, 2.35, 13) \times 2\pi$ MHz are reachable for the system consisting of the NV center in diamond and microtoroidal cavity[35]. The related Purcell factor F_p is on the order of 1×10^3, and thus, the fidelities may be close to 1 with the relevant solid state cavity-QED parameters. On the other hand, the schemes might work in the repeated-until success fashion, since photon loss and detector inefficiency in the experiment are unavoidable. The dephasing time of NV centers can be on the order of milliseconds at room temperature[11], and entanglement can be generated within the time scale of coherence time when a highly efficient single-photon source generating 1×10^4 photons per second is applied[35].

In summary, we have theoretically investigated multipartite entanglement generation of dipole emitters in the indirectly coupled dipole-microcavity systems. Benefiting from the DIT effect and the interference between dipole-microcavity systems, high-fidelity multipartite entanglement can be generated with the present accessible technology, which may be useful for scalable QIP. As the transmission spectrum is closely related to the excitation number of dipole-microcavity systems, we only discuss the generation of three classes of multipartite entanglement (e.g., the GHZ state, W state, and Dicke state), but it may be interesting to investigate the generation of other classes of multipartite entanglement in the future.

Fig. 3. Fidelities of the three-qubit GHZ state (black solid), W state (red dashed), and Dicke state (blue dot-dashed) against the Purcell factor of the dipole-microcavity system.

References

1. A. Karlsson and M. Bourennane, Phys. Rev. A **58**, 4394 (1998).
2. M. Hillery, V. Buzek, and A. Berthiaume, Phys. Rev. A **59**, 1829 (1999).
3. P. W. Shor, Phys. Rev. A **52**, R2493 (1995).
4. C. H. Bennett, D. P. DiVincenzo, J. A. Smolin, and W. K. Wootters, Phys. Rev. A **54**, 3824 (1996).
5. W. Dür, G. Vidal, and J. I. Cirac, Phys. Rev. A **62**, 062314 (2000).
6. R. H. Dicke, Phys. Rev. **93**, 99 (1954).
7. A. R. Usha Devi, R. Prabhu, and A. K. Rajagopal, Phys. Rev. Lett. **98**, 060501 (2007).
8. M. Bourennane, M. Eibl, S. Gaertner, N. Kiesel, C. Kurtsiefer, and H. Weinfurter, Phys. Rev. Lett. **96**, 100502 (2006).
9. N. Kiesel, C. Schmid, G. Toth, E. Solano, and H. Weinfurter, Phys. Rev. Lett. **98**, 063604 (2007).
10. S. Sun, H. Kim, G. S. Solomon, and E. Waks, Nat. Nanotech. **11**, 539 (2016).
11. P. Neumann, N. Mizuochi, F. Rempp, P. Hemmer, H. Watanabe, S. Yamasaki, V. Jacques, T. Gaebel, F. Jelezko, and J. Wrachtrup, Science **320**, 1326 (2008).

12. E. Waks and J. Vuckovic, Phys. Rev. Lett. **96**, 153601 (2006).

13. A. Faraon, I. Fushman, D. Englund, N. Stoltz, P. Petroff, and J. Vuckovic, Opt. Express **16**, 12154 (2008).

14. L. Ge, L. Feng, and H. G. L. Schwefel, Photon. Res. **5**, OM1 (2017).

15. Y. Zhang, Z. Zhu, Z. H. Peng, C. Jiang, Y. Chai, and L. Tan, Chin. Opt. Lett. **16**, 012701 (2018).

16. Y. P. Gao, C. Cao, T. J. Wang, Y. Zhang, and C. Wang, Phys. Rev. A **96**, 023826 (2017).

17. X. F. Liu, T. J. Wang, and C. Wang, Opt. Lett. **43**, 326 (2018).

18. Y. Guo, L. Zhou, L. M. Kuang, and C. P. Sun, Phys. Rev. A **78**, 013833 (2008).

19. T. J. Wang, Y. Lu, and G. L. Long, Phys. Rev. A **86**, 042337 (2012).

20. C. Y. Hu, A. Young, J. L. O'Brien, W. J. Munro, and J. G. Rarity, Phys. Rev. B **78**, 085307 (2008).

21. Z. H. Peng, J. Zou, X. J. Liu, Y. J. Xiao, and L. M. Kuang, Phys. Rev. A **86**, 034305 (2012).

22. T. Liu, G. Lin, F. Zhou, L. Deng, S. Gong, and Y. Niu, Chin. Opt. Lett. **15**, 092702 (2017).

23. C. Cao, X. Chen, Y. W. Duan, L. Fan, R. Zhang, T. J. Wang, and C. Wang, Sci. China-Phys. Mech. Astron. **59**, 1003155 (2016).

24. R. Zhao and R. Liang, Chin. Opt. Lett. **14**, 062701 (2016).

25. H. Kim, R. Bose, T. C. Shen, G. S. Solomon, and E. Waks, Nat. Photon. **7**, 373 (2013).

26. Z. H. Peng, L. M. Kuang, J. Zou, Y. Q. Zhang, and X. J. Liu, Quantum Inf. Process. **14**, 2833 (2015).

27. C. Y. Hu, W. J. Munro, J. L. O'Brien, and J. G. Rarity, Phys. Rev. B **80**, 205326 (2009).

28. J. H. An, M. Feng, and C. H. Oh, Phys. Rev. A **79**, 032303 (2009).

29. F. Mei, Y. F. Yu, X. L. Feng, Z. M. Zhang, and C. H. Oh, Phys. Rev. A **82**, 052315 (2010).

30. Q. Chen, W. Yang, M. Feng, and J. Du, Phys. Rev. A **83**, 054305 (2011).

31. R. J. Thompson, G. Rempe, and H. J. Kimble, Phys. Rev. Lett. **68**, 1132 (1992).

32. D. F. Walls and G. J. Milburn, *Quantum Optics*, 2nd ed. (Springer, 2008).

33. H. Rokhsari and K. J. Vahala, Phys. Rev. Lett. **92**, 253905 (2004).

34. Y. C. Liu, Y. F. Xiao, B. B. Li, X. F. Jiang, Y. Li, and Q. Gong, Phys. Rev. A **84**, 011805(R) (2011).

35. M. Hijlkema, B. Weber, H. P. Specht, S. C. Webster, A. Kuhn, and G. Rempe, Nat. Phys. **3**, 253 (2007).